Pion production and distribution in grazing relativistic heavy-ion collisions: A Monte Carlo method

Hafez M. A. Radi

Physics Department, Faculty of Science, Kuwait University, Kuwait and Nuclear Science Division, Lawrence Berkeley Laboratory, University of California, Berkeley, California 94720

Rami A. Mehrem*

Physics Department, Faculty of Science, Kuwait University, Kuwait

John O. Rasmussen

Nuclear Science Division, Lawrence Berkeley Laboratory, University of California, Berkeley, California 94720 (Received 1 August 1988)

Lorentz-invariant cross sections for the production of π^0 , π^+ , and π^- have been investigated, for the pion c.m. momentum range 0-0.5 GeV/c at angles 0°-90°, by Monte Carlo methods for grazing nuclear collisions of $^{207}\text{Pb} + ^{207}\text{Pb}$ at 0.4 GeV/nucleon. Pions are considered to be produced isotropically at the center of mass at closest approach at random from a Gaussian momentum distribution. The pion equations of motion are solved including the electromagnetic effects due to the projectile and target ^{207}Pb nuclei. The trajectory calculations differ from some earlier theoretical work in that pions are considered to scatter from the surface of, and propagate within, a spectator fragment. After surface scattering, the trajectory calculations continue but are weighted by the pion reflectivity. For that purpose, a model developed by Mehrem et al., for the relativistic oblique incidence of pions on nuclear matter represented by a uniform complex nuclear potential, has been used to evaluate the pion reflectivity for the three types of pions.

I. INTRODUCTION

Pion production is a topic of major interest in the study of medium-energy heavy-ion collisions (MEHIC). Particularly, pion emission patterns are a probe in understanding the heavy-ion reaction mechanisms. To study the behavior of hot compressed nuclear matter, heavy nuclei must be the collision partners, where the pion spectra are subject to a large Coulomb interaction.

A large amount of experimental data concerning MEHIC and inclusive, or multiplicity-tagged pion spectra have become available. 1-13 These pion spectra were measured for a variety of target-projectile incident energy combinations over a wide range of observed energies and angles. Several models have been proposed to describe these MEHIC mechanisms such as the one-fireball, 14 these MEHC mechanisms such as the one-fireball, two-fireball, ¹⁵⁻¹⁷ firestreak, ¹⁸ row-on-row, ¹⁹ hydrodynamical, ²⁰⁻²³ statistical thermodynamical, ²⁴⁻²⁸ and the intranuclear cascade. ^{20,29-32} The Coulomb effects ³³⁻⁴² and reabsorption or scattering can modify the pion emission patterns depending upon the impact parameter of the heavy-ion collisions. In most of the the theoretical studies³⁵⁻³⁸ of Coulomb effects on pions the trajectories have been allowed explicitly or implicitly to propagate through nuclear matter. On the other hand, Monte Carlo studies by Radi et al., 42 differ from the earlier theoretical work³⁵⁻⁴¹ since in Ref. 42 points were considered to be absorbed if they passed within 0.8 of the radius of spectator nucleus. In all these theoretical studies only inclusive spectra were examined.

This paper is similar to Ref. 42 in that Coulomb effects on pions produced in heavy-ion reactions, using Monte Carlo methods, will also be examined. However, the present study is extended in the range of energy it covers for both the reaction energy and pion momentum, so that the treatment is made relativistic. ²⁰⁷Pb nuclei are chosen for the collision in this study. While the more usual beams may be ²⁰⁸Pb, the targets are natural Pb with average atomic weight 207. The difference between mass 207 and 208 is insignificant.

For this paper we simplify the problem by limiting the study to grazing collisions. Thus, a specific model (cascade, fireball, firestreak, etc.) describing the nucleons in the overlap region is not needed in this study. This is a useful step, since it removes the complications of averaging over impact parameters and of using an uncertain model for a source function. The pion is assumed to start its "journey" at the time and place that the projectile and target come closest to each other (here assumed somewhat arbitrarily to be surfaces at 0.4 fm minimum separation to take into account the fact that for peripheral events pions may be formed when the tails of the nuclear density distributions overlap). Also, the two nuclei are assumed to continue with unchanged velocities for such high-energy collisions.

The Coulomb effect, relativistically an electromagnetic interaction, of the two-spectator nuclei on the pion is considered in this study. This is done in the center-of-mass frame of the two colliding nuclei. A set of coupled differential equations that represent the motion of the

pion under this electromagnetic force is derived. This study differs from earlier theoretical work³⁵⁻⁴² in that pions are allowed to scatter upon hitting the spectator nuclear surface. In other works, scattering of the pion [which has been created at time t=0, as shown in Fig. 1(a), and after Coulomb deflection may strike the surface of the spectator fragment at time t, as shown in Fig. 1(b)] must be considered. In this process, a pion-nucleus interaction via the optical potential is involved.

The most recent operator form of the optical potential has been developed by Stricker et al., 43,44 and Carr et al., 45 where the pion energy is used in its relativistic form, while the massive nucleus is treated nonrelativistically. An optics approach developed by Mehrem et al. 46 is "hooked" to the model to obtain the reflectivity of the pion as it is scattered. The reflectivity here will be taken as a weight given to the scattered pion. Hence, one does not wipe out the pion upon striking the nucleus (as has been done in Ref. 42), but instead one allows it to scatter, giving it less weight in the final spectrum because the reflectivity is less than unity.

This optical potential, however, has been given in the pion-nucleus center-of-mass frame. $^{43-45}$ So, once a pion strikes the nucleus in the center of mass of the colliding nuclei, a transformation is made to the frame of the nucleus, taken to be equivalent to the pion-nucleus frame, and the optical potential is turned on. The reflectivity is then calculated and a transformation is again made back to the center-of-mass frame of the colliding nuclei; the pion then continues its trajectory but with less weight. An approximation has been made in implementing the optical potential operator form, which is setting the density of the nucleus to be constant; it is taken to be the density at the center of the nucleus, ρ_0 =0.17 nucleons/fm³. This has been done to avoid mathematical complications.

Section VI is completely devoted to the Monte Carlo results. The double differential cross sections for the three types of pions are presented as a function of pion final momentum and scattering angle.

II. PION-NUCLEUS INTERACTION AND ITS OPTICS APPROACH

The scattering of a pion, via an optical potential operator, from a massive nucleus of mass number A and charge Z is a point of interest at this stage. This potential operator consists of two terms. The first term is a

single-particle potential which is local in configuration space and represents the interaction between the pion and the nucleus. The second term represents scattering which proceeds through an intermediate excited state of the nucleus and is nonlocal in configuration space.⁴⁷

The formalism of multiple-scattering theory has been worked out in the early 1950's especially by Watson⁴⁸ and by others,⁴⁹ and is essentially a nonrelativistic approach. On the other hand, analysis of the data of pionic atoms, as well as the scattering of the pion by many nucleons of the nucleus, has led to certain convenient approximations and parametrizations in the multiple-scattering theory. These approximations have been introduced by Ericson and Ericson⁵⁰ for the local part of the optical potential. The nonlocal term is introduced by Kisslinger⁵¹ for low-energy pion-nucleus scattering.

The recent second-order, semirelativistic, optical potential operator form developed by Stricker et al., 43,44 and Carr et al., 45 is used in our work. Formally, for a nucleus of Z protons, N neutrons, mass number A, and nuclear density $\rho(r)$, the optical potential operator, $\tilde{U}_{\rm opt}$ can be written in a convenient form as given by Ref. 46.

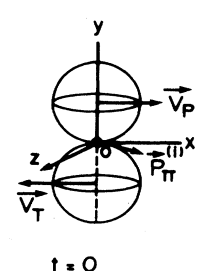
In the evaluation of $U_{\rm opt}(r)$, $\rho(r)$ has been set constant and equal to $\rho(0) = \rho_0$, the nuclear density at the center of the nucleus, where $\rho_0 = 0.17$ nucleons/fm³. A theoretical set of parameters (named set C in Carr's recent dissertation⁵² and presented in Table I of Ref. 46) that gives a smooth variation of the parameters with pion incident energy is considered here. A fit of the lower part of Fig. 1 of Ref. 46 and similar one for each charged pion is done to recreate k_1 and k_2 for any incident value of k_0 and can be generally written (for the three types of pion) as

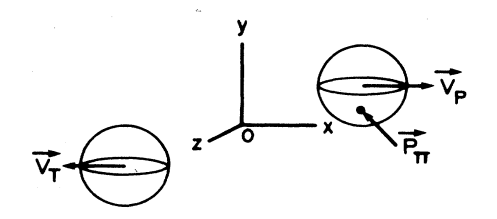
$$k_1 = a_0 + a_1 k_0 + a_2 k_0^2 + a_3 k_0^3 ,$$

$$k_2 = b_0 + b_1 k_0 + b_2 k_0^2 + b_3 k_0^3 ,$$
(1)

where the coefficients are given in Table I for the various ranges of pion kinetic energy T. For incident kinetic energies larger than 180 MeV, the behavior for k_1 is assumed to continue rising, while that for k_2 to continue decreasing.

For an obliquely incident plane wave on a nuclear surface assumed to be sharp, as shown in Fig. 3 of Ref. 46, the solutions of the Klein-Gordon equation in the two regions can be obtained. Then, application of the boundary conditions of continuity of the wave function and its derivative leads to





at time t

FIG. 1. Schematic diagram showing the creation of the pion with initial momentum, $\mathbf{P}_{\pi}^{(t)}$, between the two colliding nuclei at time t=0. Also, shown is the possible collision of a pion with one of the two nuclei at a later time t in the center of mass frame.

T (MeV)	Type of pion	a_0	a_1	a_2	a_3	b_0	b_1	b_2	\boldsymbol{b}_3
0-67		0.0278	0.2649	1.39	0	0.5138	-2.147	3.666	-11.419
> 67-130	π^0	0.7916	1.901	-3.886	1.26	0.3903	1.245	1.255	-4.539
> 130-180		0.9864	0.3177	-1.9597	3.9933	0.7986	0.4999	-1.4946	0
0-67		0.01379	0.1149	1.39	0	0.5941	-1.848	2.165	-0.1914
> 67-130	π^-	0.6865	2.23	-4.533	1.584	0.3715	1.328	1.016	-4.135
> 130-180		0.9286	0.3738	-2.3003	4.4221	0.8002	0.5662	-1.446	0
0-67		0.06228	0.7916	0.7202	0	0.3844	-1.74	3.409	-1.486
> 67-130	π^+	0.8847	1.688	-3.469	1.132	0.3912	1.207	1.534	-5.111
> 130-180		1.055	0.2514	-1.5429	3.4215	0.7924	0.444	-1.597	0

TABLE I. Coefficients for fitting k_1 and k_2 as a function of k_0 for the three types of pions.

$$\frac{\sin\theta_0}{\sin\theta} = \frac{k_1 + ik_2}{k_0} \tag{2}$$

and

reflectivity =
$$|R|^2 = \left| \frac{\sin(\theta - \theta_0)}{\sin(\theta + \theta_0)} \right|^2$$
. (3)

III. DYNAMICS OF THE MODEL

The aim of this section is to find the electromagnetic force exerted by the two moving spectator nuclei on a moving pion.

Now let the motion of a charged pion be considered in the field of the two nuclei, namely the projectile and the target (P and T), in frame S (center of mass). The approach to the problem will be as follows: At any instant t, in frame S, the pion has velocity \mathbf{u} and position \mathbf{r} (variables with no subscript will only describe the pion unless specified, hereafter). The center of the nucleus under consideration has a velocity \mathbf{v}_j and position \mathbf{r}_j (j=P,T), respectively. The pion can be considered as being instantaneously moving with velocity \mathbf{u}_0 at position \mathbf{r}_0 with respect to a frame S_0 that has a velocity \mathbf{v}_j with respect to S. We transform to S_0 using the Lorentz transformations. In S_0 the nucleus under consideration is at rest, and hence its position at any moment is the same. This

specifies that \mathbf{r}_{j_0} - \mathbf{r}_0 is the distance between the pion and the center of the nucleus occurring at the same time.

Generally, the force exerted by nucleus j on a pion in frame S can be obtained by transforming back from frame S_0 to frame S using the inverse Lorentz transformation and can generally (after some algebraic manipulation) be written as

$$\mathbf{F}_{j\pi} = q_{\pi}(\mathbf{E}_{j} + \mathbf{u} \times \mathbf{B}_{j}) = \mathbf{F}_{j\pi}(\text{elec}) + \mathbf{F}_{j\pi}(\text{mag}) ,$$

$$(J = P, T) , \quad (4)$$

where

$$\mathbf{F}_{i\pi}(\text{elec}) = q_{\pi} q_i \gamma_i \mathbf{r}_{i\pi} / r_{i\pi}^{'3} , \qquad (5)$$

$$\mathbf{F}_{j\pi}(\text{mag}) = \frac{1}{c^2} \mathbf{u} \times \mathbf{v}_j \times \mathbf{F}_{j\pi}(\text{elec}) , \qquad (6)$$

$$\mathbf{r}_{i\pi} = \mathbf{r}_{\pi} - \mathbf{r}_{i}$$
,

$$\mathbf{r}'_{j\pi} = \mathbf{r}_{j\pi} + (\gamma_j - 1)(\mathbf{r}_{j\pi} \cdot \mathbf{v}_j) \mathbf{v}_j / v_j^2 ,$$

$$\gamma_j = 1/(1 - v_i^2 / c^2)^{1/2} = [1 + (P_j c)^2 / (m_j c^2)^2]^{1/2} ,$$

where $\mathbf{F}_{j\pi}$ denotes the force exerted by the j nucleus on the pion and $\mathbf{r}_{j\pi}$ is the vector from the j nucleus to the pion. Using dimensionless variables (denoted by a hat on the variable), the force exerted by the two nuclei on the pion is given by

$$\frac{d(\mathbf{P}_{\pi}c)}{d\hat{t}} = \frac{\varepsilon_{\pi}e^2}{D} \sum_{J=P,T} Z_j \gamma_j [\mathbf{r}_{j\pi} + (\mathbf{P}_{\pi}c) \times (\mathbf{P}_{\pi}c) \times \mathbf{r}_{j\pi} / (\gamma_{\pi}m_{\pi}c^2\gamma_j m_j c^2)] / (\hat{r}'_{j\pi})^3$$
(7)

where

$$\hat{t} = t/T$$
, with $T = \frac{1}{3} \times 10^{-23}$ sec,
 $\hat{r} = r/D$, with $D = 1$ fm,
 $D/T = c$, with $c = 3 \times 10^{23}$ fm sec⁻¹,

 $\varepsilon_{\pi} = \pm 1$, for the positive and negative charged pions, re-

spectively, and ε_{π} =0 for neutral ones. In Eq. (7), \mathbf{P}_{π} is the pion momentum in MeV/c, as measured in frame S, then \mathbf{P}_{π} = $\gamma_{\pi}m_{\pi}\mu$.

Now, the general equation, Eq. (7), will be applied to the case of interest. The case here is, as mentioned before, the grazing collision (impact parameter, $b=2R_0$) of two symmetric nuclei ($m_p=m_T=M$, $Z_p=Z_T=Z$) of ^{207}Pb , producing a pion at their point of interaction.

Hence, the force on the pion due to the two nuclei will differ, from one to the other, in that algebraic signs of their velocities and coordinates will be opposite. In this case

$$\beta_p = \beta_T = 1/[1 + 2M_N c^2/\epsilon_k]^{1/2} = \beta^* ,$$

$$\gamma_p = \gamma_T = \gamma^* ,$$

with $(M_N c^2 \simeq 931 \text{ MeV})$. Also, for a symmetric system we have

$$\mathbf{P}_{p}c = \gamma^* M c^2 \beta^* \mathbf{e}_{x} = -\mathbf{P}_{T}c ,$$

where e_x is a unit vector along the x axis. Therefore, the equations of motion of the pion can be written in the following form of first-order coupled differential equations:

$$\begin{split} \frac{d\hat{\mathbf{r}}}{dt} &= \hat{\mathbf{u}}_{x} , \\ \frac{d(P_{x}c)}{d\hat{t}} &= \frac{Z\varepsilon_{\pi}e^{2}\gamma^{*}}{D} \sum_{n=-1,1} \left[(\hat{x} + n\beta^{*}\hat{t}) - \frac{\beta^{*}n}{\gamma^{*}\mu} [P_{y}c(\hat{y} + n\hat{R}_{0}) + P_{z}c\hat{z}] \right] / \hat{r}_{n}^{'3} , \end{split} \tag{8}$$

$$\frac{d(P_{y}c)}{d\hat{t}} = \frac{Z\varepsilon_{\pi}e^{2}\gamma^{*}}{D} \times \sum_{n=-1,1} (\hat{y} + n\hat{R}_{0})[1 + n\beta^{*}(P_{x}c)/(\gamma^{*}\mu)]/\hat{r}_{n}^{'3},$$
(10)

$$\frac{d(P_zc)}{d\hat{t}} = \frac{Z\epsilon_\pi e^2 \gamma^*}{D} \sum_{n=-1,1} \hat{z} [1 + n\beta^* (P_xc/\gamma^*\mu)] / \hat{r}_n^{'3},$$
 where

$$\hat{r}'_{n} = \{ [\gamma^{*}(\hat{x} + n\beta^{*}\hat{t})]^{2} + (\hat{y} + n\hat{R}_{0})^{2} + \hat{z}^{2} \}^{1/2}$$

$$(n = -1, +1) .$$

Once Eqs. (8)–(10) are solved together, they produce the pion momentum components and the x, y, and z coordinates as a function of time, provided the initial conditions are known. This system of coupled first-order differential equations is integrated using the modified Adams-Moulton predictor-corrector method until the pion velocity becomes almost constant. For the case of neutral pions, it is possible to treat it separately. This is done to save computer time and is described in Ref. 53.

So far, the nuclei have been treated as point particles, since in the electromagnetic interaction only the positions of their centers are involved. However, when the pion collides with the nucleus, its geometrical shape becomes of interest, and it is necessary to find the reflectivity. If the pion coordinates (x, y, z, z), at a particular instant) satisfy⁵³

$$\gamma_i^2 (x - x_i)^2 + (y - y_i)^2 + z^2 = R_0^2$$
, (12)

then its scattering must be considered. To do this, one

has to make a transformation from frame S to frame S_0 for the variables describing both the pion and the nucleus under consideration, to determine both the momentum and angle of incidence in the rest frame of the nucleus.

IV. SCATTERING OF A PION FROM A MOVING NUCLEUS

The reflectivity of the pion upon scattering from a moving nucleus will be obtained in terms of the ratio of the outgoing and incoming current densities. The procedure is to transform, relativistically, the current density from frame S to frame S_0 , allow the pion to scatter, then transform it back to frame S.

When Eq. (12) holds, the first step is to transform from frame S (the center-of-mass frame of the colliding nuclei) to frame S_0 (rest frame of the nucleus) for the variables describing both the pion [as the momentum \mathbf{P} , position \mathbf{r} , incident wave $\psi_{\rm in}(\mathbf{r},t)$, and the current density $\mathbf{J}_{\rm in}(\mathbf{r},t)$], and the nucleus (as the momentum \mathbf{P}_j and the position \mathbf{r}), with which the pion is colliding. This will determine the pion momentum, the current density and the angle of incidence in the rest frame of the nucleus.

After maintaining the plane wave $\psi_{\rm in}^{(0)}({\bf r}_0,t_0)$ and its corresponding current density ${\bf j}_{\rm in}^{(0)}({\bf r}_0,t_0)$ in S_0 , the next step is to allow this plane wave to scatter from the nuclear surface. To do this a technique has to be developed in order to find the direction of propagation of the scattered wave in a calculable mathematical form. This technique is described in Ref. 53. Also, using this technique, the angle of incidence θ_0 as well as the reflected pion momentum ${\bf P}_0$, can be obtained. In order to use the method developed by Mehrem et al., ⁴⁶ for an obliquely incident plane wave on a sharp nuclear surface, we need a reflected wave of the form

$$\psi_{\text{sc}}^{(0)}(\mathbf{r}_0, t_0) = R e^{i(\mathbf{P}_0' \cdot \mathbf{r}_0 - E_0 t_0)/\hbar}, \text{ with } P_0' = P_0,$$
 (13)

where the sc subscript denotes the scattered wave and R is the reflection amplitude. Hence, the current density of the reflected wave will be

$$\mathbf{j}_{\text{sc}}^{(0)}(\mathbf{r}_0, t_0) = |R|^2 \mathbf{P}_0' / m(\mathbf{P}_0') . \tag{14}$$

At this point, the reflectivity measured in frame S_0 is given by

reflectivity =
$$|j_{sc}^{(0)}/j_{in}^{(0)}| = |R|^2$$
, (15)

where $|R|^2$ is given by Eq. (1). Knowing θ_0 and P_0 (= $\hbar k_0$), one can determine, using Eqs. (1) and (2), θ , which can then be used in Eq. (1) to evaluate $|R|^2$.

In moving back from S_0 to S, $\psi_{sc}^{(0)}$ in S_0 will transform similar to Eq. (13), but with the omission of the superscript and the subscript 0. Its corresponding current density will be

$$\mathbf{j}_{sc}(\mathbf{r},t) = |R|^2 \mathbf{P}' / m(P') , \qquad (16)$$

where P' is obtained by applying the inverse Lorentz transformations of P'_0 from S_0 to S (Ref. 53).

Finally, the ratio of the currents \mathbf{j}_{sc} to \mathbf{j}_{in} determine how much is being reflected out of the incident pion upon scattering from the moving nucleus. Hence,

reflectivity =
$$|j_{sc}/j_{in}|$$

= $F(P,P')|R|^2$, (17)

where the reflectivity form factor F is given by

$$F(P,P') = P'[1 + (Pc)^2/\mu^2]^{1/2} / \{P[1 + (P'c)^2/\mu^2]^{1/2}\}.$$
(18)

V. SAMPLES OF PION TRAJECTORIES

So far, two aspects affecting the pion trajectory have been discussed; they are the electromagnetic effects due to the two nuclei, and the scattering of the pion due to the collision, if any, with one of them. Now as the pion continues on its trajectory, it can be affected by either one of these two aspects, both or neither (for the case of π^0). Their occurrence depends on the type of pion one is studying, the initial conditions with which one starts the pion trajectory, and the kinetic energy per nucleon of the projectile and target nuclei in the center-of-mass frame.

Each of the two ²⁰⁷Pb nuclei, from now on, will be considered as having a kinetic energy of approximately 95 MeV/nucleon in the center-of-mass frame. To take into account the fact that for peripheral events pions may be formed when the tails of the nuclear density distributions overlap, the two nuclear surfaces have been given a separation distance of 0.4 fm along the y axis at t = 0, and the pion is created at the origin [Fig. 1(a)].

In this section, two samples of pion trajectories are studied for both π^+ and π^- . For each sample of π^+ and π^- , a set of graphs will be introduced to show the variation of certain variables of the pion with time. The two examples involve starting the pion with initial momentum components $P_x^{(i)}=66$ MeV/c, $P_y^{(i)}=5$ MeV/c, and $P_z^{(i)}=0$. The reason for such a choice is to give the pion almost the same speed along the positive x direction as the upper nucleus so that the pion can survive in the vicinity of the upper nucleus for a longer time. Also a small momentum component along y is given to the pion for two purposes; first, it allows the pion a better chance to collide with the upper nucleus, and second the smallness of this component makes the case serve as an example of a pion that survives after a collision with the nucleus, i.e., the pion survival is always near to 1. The initial speed of the pion is $\beta_x^{(i)} \simeq 0.43$. Also the speed of the nucleus is calculated to be equal to $\beta_j \simeq 0.42$ (j=P,T).

In the first study of a π^+ the electromagnetic effect of the two nuclei (projectile and target) is given in Fig. 2. Separate calculations (not shown here) show that the survival graph yields 1 for the electric effect by itself and 0.85 for the magnetic, while on the other hand it yields 0.9 when the electromagnetic effect is considered. This is due to the repulsion of the upper nucleus to π^+ when electric effects are present, so that the pion strikes the nucleus with less momentum than it does when considering only the magnetic effect.

In the second study of a π^- the electromagnetic effects due to the two nuclei on π^- are shown in Fig. 3. These effects can, as in the case of π^+ , be deduced from the behavior due to electric and magnetic effects. However, in

the F_x vs t graph, the two clear drops in the force due to collisions may not have been predicted easily from electric and magnetic effects alone. In the case of the electromagnetic effect, the collision of π^- with the nucleus has been delayed a bit (as compared with π^+), as seen from the F_x graphs. This delay has been caused by the magnetic positive force along x. Once the collision actually takes place, the y component of the pion momentum reverses its direction. This results in making the positive x component of the magnetic force negative; hence, the total force along x becomes, at collision, more negative, as shown by the clear drop in the force graph. The same analysis applies for the second collision.

For π^0 the only cause of change in the motion is the collision with one of the two nuclei.

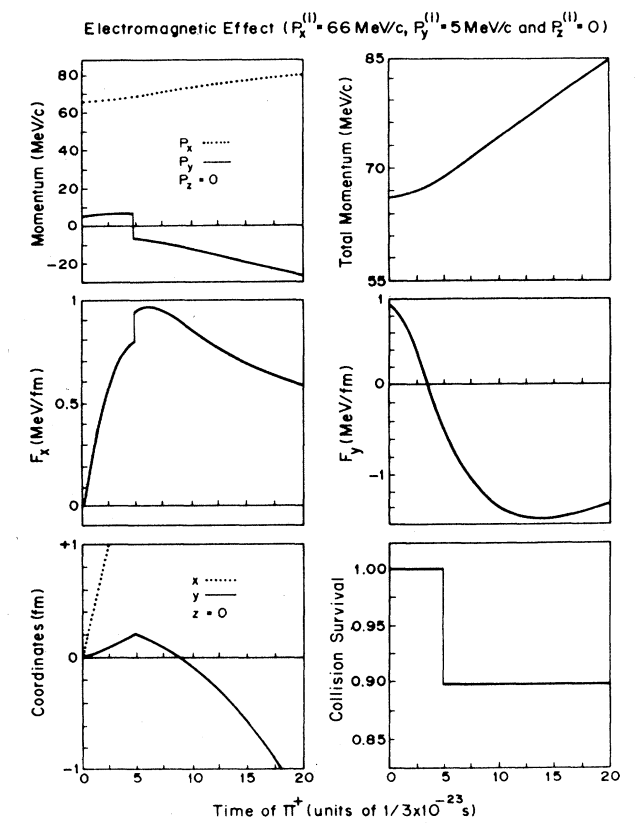


FIG. 2. Set of plots showing only the electromagnetic effect on π^+ due to the presence of the projectile and target nuclei $[^{207}\text{Pb} + ^{207}\text{Pb}$, grazing collision], viewed in the center-of-mass frame. The pion initial momentum components for this figure are $P_x^{(i)} = 66 \text{ MeV/c}$, $P_y^{(i)} = 5$, and $P_z^{(i)} = 0$. Time zero is taken as the time when the two nuclei are at the distance of closest approach, in the center-of-mass frame. This figure includes plots describing the variables: Pion momentum components along x and y where the pion momentum along z is zero, pion total momentum, the forces along x and y acting on the pion due to the projectile and target nuclei, pion coordinate components along x and y where the pion has no motion along z, and the pion reflectivity (collision survival).

VI. RESULTS AND DISCUSSION

A. The Monte Carlo calculation

The aim of this section and the following one is to describe the calculation of the differential cross section for the pion spectrum resulting from a grazing collision of two ²⁰⁷Pb nuclei in the center of mass. The cross section is obtained by a method that makes the procedure very similar to the procedures of the actual experiment.

A Monte Carlo run involves starting the pion with different set of initial conditions, chosen from the specified distributions, a large number of times. The pion initial momentum is chosen randomly such that P_x , P_y , and P, are each chosen from a Gaussian distribution, representing a Boltzmann distribution. These initial distributions are shown in the left uppermost graphs of Figs. 9, 10, and 11, respectively, in Ref. 53. In this study a total of about 200 000 trials were made. However, not all of these trials initiated a trajectory calculation, for there is a restriction on pion initial total momentum to be not more than about 700 MeV/c. The chronological order of events is that the pion starts its trajectory at time t=0, with randomly chosen momentum components, then it either escapes or makes collisions. Its final momentum is recorded when it does not change appreciably, or if the set time limits are exceeded. The set time limit for π^+ and π^- is $t=30\,000T$, and for π^0 it is t=1000T, where $T=\frac{1}{3}\times 10^{-23}$ sec (the lifetime for π^+ and π^- is

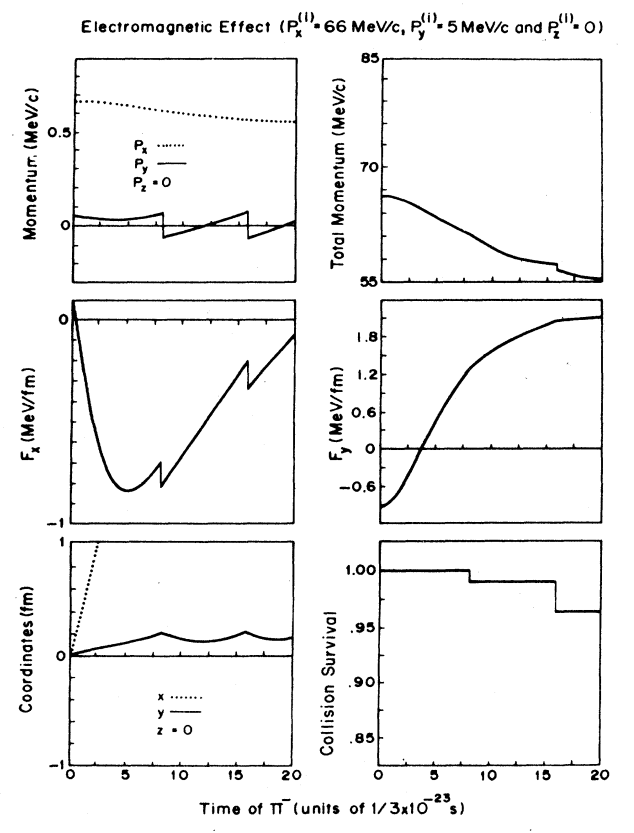


FIG. 3. Same as Fig. 2, but for the electromagnetic effect on π^- .

 2.6×10^{-8} sec and the lifetime of π^0 is 8.4×10^{-17} sec). The Adams-Moulton predictor-corrector routine checks on the pion position in steps of time. In this code these steps of time have been made variable according to how far the pion is from either of the two nuclei. In other words, if the pion is found far from the nuclei, the code integrates in larger steps than if it had been closer. The code terminates the pion trajectory once its momentum changes by less than about 0.001%. However, this termination is turned off when t < 10T, to allow for a possible small change of its momentum while the pion is still close to one of the two nuclei. As the pion is finally counted, it is weighted by its final survival from surface reflections. Starting the pion with survival fraction 1, i.e., with maximum weight to the cross section, the final survival is calculated by successively multiplying the survival fraction of the pion by its previous value as the pion makes another collision. Naturally, if the pion makes no collisions, its final survival is taken to be 1. Mainly, two more restrictions are introduced here to save lengthy computer time and are discarded later on in the calculations. They are to stop the pion trajectory if the pion makes more than 10 collisions or reaches a survival less than 0.1. This is thought to be useful in saving time since a pion with such "history" does not add to the calculated cross section; in most cases this rejected pion has a survival of almost zero. However, some pions have been found to stay with a survival factor just above 0.1 during the first ten collisions.

Figure 4 shows the histograms for the pion final number of collisions during its trajectory for π^0 , π^+ , and π^- . The figure shows the distribution of the pions that make at most four collisions, where the pions that make more than four collisions are insignificantly small in number. The first step in the graphs of Fig. 4 indicates the number of pions ending with no collisions, the second for the ones ending with one collision, etc. Each bin, naturally, has the size of one collision. As expected, the ones ending with no collisions have the highest occurrence for the three types of pions. More features of the graph are explained in Ref. 53.

Figure 5 shows the histograms for pion final survival for π^0 , π^+ , and π^- . Each bin of survival has the size of 0.2. It is apparent from the figure that the highest occurrence is for pions ending their trajectories with high survival factors. In addition, it is observed that fewer negative pions have high survival factors relative to positive and neutral pions. This is due to the tendency of the negative pions to remain around the nucleus, resulting in more collisions and lower survival as mentioned previously. The main peak showing for π^0 , π^+ , and π^- has a different width for each type of pion. It has the highest width for π^+ and, on the other hand, the lowest width for π^-

B. Pion-invariant cross-section spectrum

The Lorentz-invariant differential cross section is

$$E_{\pi} \frac{d^3 \sigma}{dP^3} \equiv \frac{E_{\pi}}{P^2} \frac{d^2 \sigma}{dP \, d\Omega} \, , \tag{19}$$

where dP^3/E_{π} is the Lorentz-invariant phase-space

volume, and E_π and P are the pion total energy and momentum, respectively. Furthermore, the differential element of solid angle, $d\Omega$, is given, in spherical coordinates, by

$$d\Omega = \sin\theta \, d\theta \, d\phi \, . \tag{20}$$

Hence, integrating Eq. (19) over ϕ , to compare with the experimental results, one obtains

$$\int E_{\pi} \frac{d^3 \sigma}{dP^3} d\phi \equiv E_{\pi} \frac{\Delta N}{\Delta V} , \qquad (21)$$

where ΔN is the number of pions whose momenta lie between $P-\Delta P$ and $P+\Delta P$ and whose scattering angles lie between $\theta-\Delta\theta$ and $\theta+\Delta\theta$. Also, ΔV is the volume enclosed by two spherical sectors of radii $P-\Delta P$ and $P+\Delta P$. The spherical sector is formed by the rotation of a sector about the beam axis. This sector has a central angle $2\Delta\theta$ and a bisector that makes an angle θ with the beam axis. So.

$$\Delta V = \frac{2}{3}\pi[(P+\Delta P)^3 - (P-\Delta P)^3]$$

$$\times [1-\cos(\Delta\theta)], \text{ for } \theta=0,$$

$$\Delta V = \frac{2}{3}\pi[(P+\Delta P)^3 - (P-\Delta P)^3]$$

$$\times [\cos(\theta-\Delta\theta) - \cos(\theta+\Delta\theta)], \text{ for } 0^\circ < \theta < 90^\circ,$$

$$\Delta V = \frac{2}{3}\pi[(P+\Delta P)^3 - (P-\Delta P)^3]$$

$$\times [\sin(\Delta\theta)], \text{ for } \theta=90^\circ.$$
(22)

Furthermore, $\Delta\theta$ is taken to be 5° and P to be 10 MeV/c, where the values are comparable to the values used for the experimental resolution in Ref. 2.

When the pion has finally survived with a factor greater than 0.1 and a number of collisions less than ten, then its total momentum will decide in which bin this pion will be counted. Once the right bin is found, the pion will be binned with a weight equal to its survival factor. If another pion has a final total momentum that makes it lie in the same bin, then its weight will be added to the weight recorded earlier in this bin. This accumulation of pion weight produces the number ΔN when the procedure of binning is over. So, each bin has its own value of ΔN for a given type of histogram. One can determine the cross section versus pion final total momentum for the different pion scattering angles by applying Eq. (21). Similarly, the cross section versus pion scattering angle, for the different pion final momenta, is determined.

The range of the pion final total momentum used here is $0 \le P \le 500$ MeV/c, while the range of the pion scattering angle is $0^\circ \le \theta \le 90^\circ$. For a momentum distribution (with a fixed angle, $\theta_s = 0^\circ, 10^\circ, \ldots, 90^\circ$), the momentum range is divided into 25 bins with each bin having a width of 20 MeV/c. The value of the momentum for each bin is determined at its center. On the other hand, for an angular distribution (with a fixed momentum, $P_s = 0, 50, \ldots, 450$ MeV/c), the angular range is divided into nine bins with each bin having a width of 10° . The value of the angle for each bin is determined at its center. In the case of the momentum distribution histograms, if

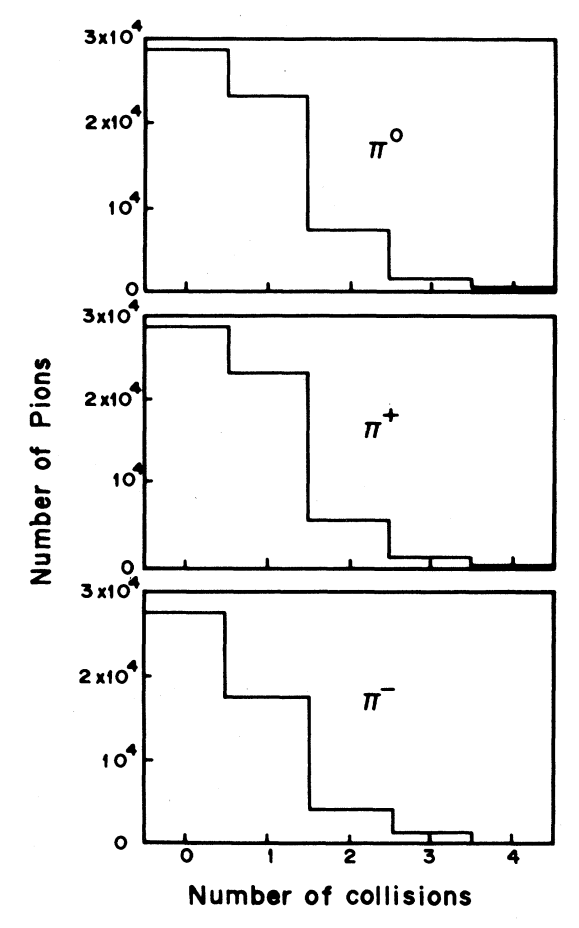


FIG. 4. Histograms for pion final number of collisions, applied for π^0 , π^+ , and π^- .

the pion is found between scattering angles $\theta_s - \Delta \theta \le \theta \le \theta_s + \Delta \theta$, where $\Delta \theta = 5^\circ$ as given before, then its scattering angle is taken to be θ_s . For the angular distribution histogram, if the pion is found between $P_s - \Delta P \le P \le P_s + \Delta P$, where $\Delta P = 10$ MeV/c as given before, then its final momentum is taken to be P_s .

At this point one may notice that the number of studied positive pions, for example, differs from the number of studied negative or neutral pions. How, then, can one compare between the results for the three types of pions? Sullivan, 2,55 following Sternheim and Silbar, 56 using Clebsch-Gordan branching relations for Δ decay has given Eqs. (6.8) and (6.10), in Ref. 55, from which the primitive π^-/π^+ ratio is given. However, this study is not intended to analyze the differences between the cross sections for π^- and π^+ ; hence, that weighting factor has not been used in the calculations of the cross section. The cross sections are normalized arbitrarily, by a multiplicative factor for the three types of pions, as there are no experimental results that one can compare these theoretical cross sections against. The scale used for the cross section is, naturally, logarithmic for proper representation of the results. Moreover, the symmetry of the system of projectile and target in the center of mass makes it unnecessary to show the cross sections for an-

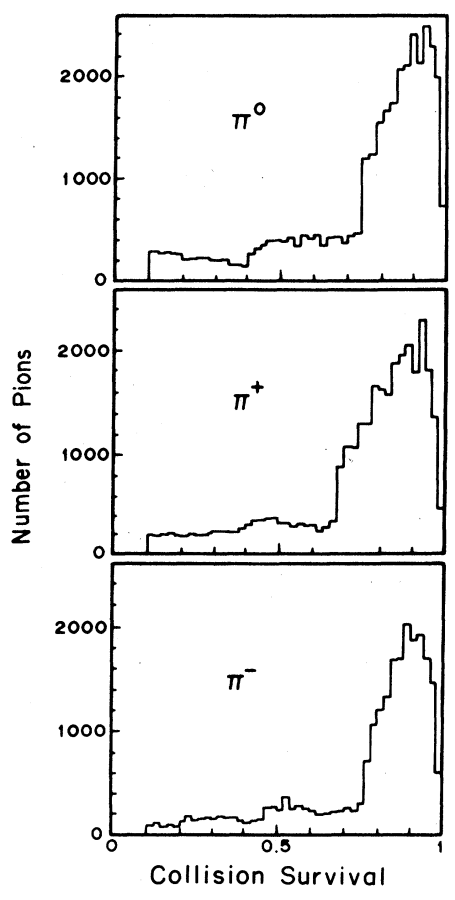


FIG. 5. Histograms for pion final survival applied for π^0 , π^+ , and π^- . Pions with $|R|^2=1$ (i.e., pion experiencing no collisions) are not shown.

gles outside the range $0^{\circ} \le \theta \le 90^{\circ}$. Moreover, vertical bars are introduced in the cross section figures, as they are an indication of the statistical errors of these cross sections.

Figures 6-8 show plots of the Lorentz-invariant cross sections versus momentum at fixed center-of-mass angles from 0° to 90° for π^0 , π^+ , and π^- . (A preview of these results was presented earlier.⁵⁷) The general trend observed in these figures is a decrease in the cross section as the angle is increased, for pion momentum higher than about 250 MeV/c. The cross section versus momentum graph for π^0 , Fig. 6, shows that the maximum cross section has remained, for all angles, in the momentum range of the first few bins. For final momenta beyond these bins, the graph smoothly decreases as the momentum is increased. Moreover, it is observed that in this figure, and the two to follow, the statistical error bars in the momentum range of the last few bins for some angles disappear. This indicates that a large error bar must be drawn at these bins with low values of the cross section. As for the cross section versus momentum for π^+ , Fig. 7, the graph shows that for forward scattering angles, no pions exist with final momenta less than 200 MeV/c. This is best explained as being caused by the neglect of quantum effects. Also, since our code starts the π^+ with at least the zero

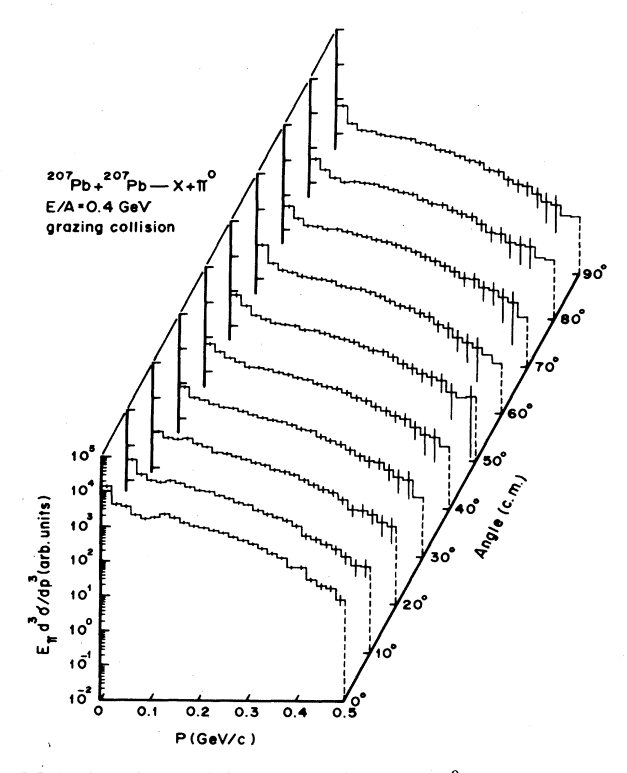


FIG. 6. Differential cross sections for π^0 resulting from a grazing collision of two ²⁰⁷Pb nuclei in the center-of-mass frame. The cross section is given as a function of pion final momentum at the forward scattering angles $0^{\circ}, 10^{\circ}, \dots, 90^{\circ}$.

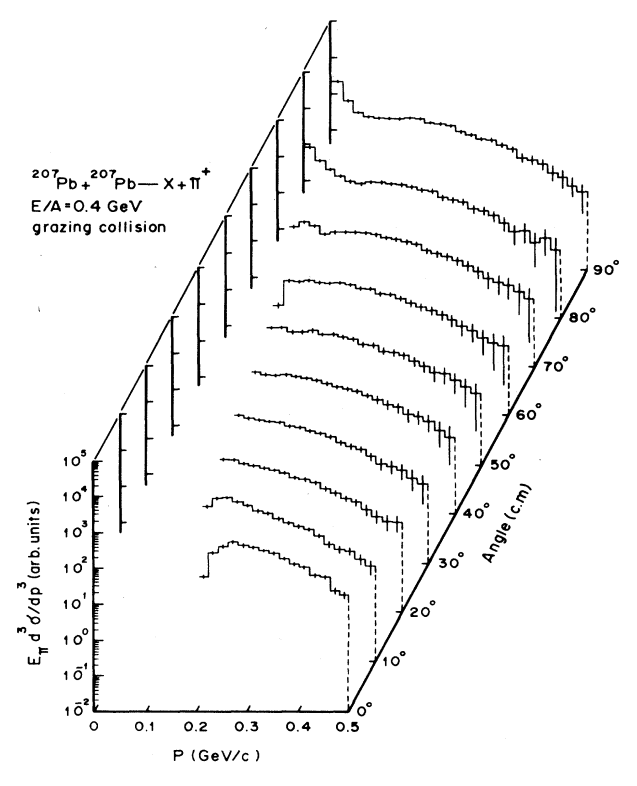


FIG. 7. Same as Fig. 6, but for π^+ .

momentum at the point where the two nuclei almost "touch," then the total energy of π^+ will be at least the sum of potential energies of both projectile and target, U_0 . Hence, for forward angles, positive pions will acquire energy at least greater than U_0 . To have π^+ with energy less than U_0 we should start the pion with an energy, E_0 , less than U_0 and let it tunnel through the barrier to a large distance where $E_0 = U(r_f)$. The region around π^+ projectile or target velocity will be most sensitive to the neglect of these slow moving pions. Only at 80° and 90° are positive pions found in all bins of momenta. For momenta less than about 250 MeV/c, the general trend is that of increasing cross section as the angle is increased. This is clearly seen from 70° to 90°. This trend is similar to an observation in the work of Wolf et al. 1 where the heaviest collision studied is ²⁰Ne+²³⁸U at 0.4 GeV/nucleon, so it is not really comparable in Coulomb interaction to our Pb on Pb. Their Fig. 7(b) shows a continuous and gently peaked distribution for π^+ with a cross section increase for low-energy pions as the angle is increased. It may be misleading to compare the lowenergy part of the cross section of the present work with the inclusive experimental cross section of Wolf et al. 1 However, this comparison can be made possible as follows: In the study of pion production from the collision of medium-energy protons on heavy-target nuclei, 56,58,59 it is generally concluded that the π^+ originates predominantly from proton-proton collisions at the nuclear surface. Thus, one may expect a similar behavior by just comparing the experimental inclusive cross section with

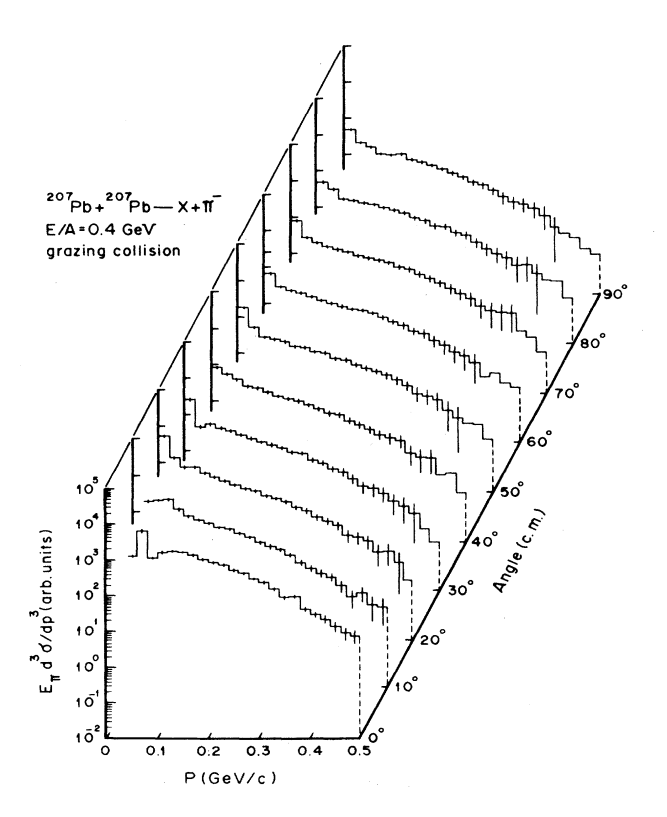


FIG. 8. Same as Fig. 6, but for π^- .

the grazing collision cross section of the present study, only at low energy. Also, in both cases pions start at the nuclear surface. The cross section versus momentum for π^- , Fig. 8, indicates that at scattering angles less than 20°, no negative pions are found with final momenta between 0 and 20 MeV/c. A distinguishable peak appears at projectile, or target, velocity for the forward scattering angle. The general trend looks, more or less, like the one in Fig. 11 of the work of Nagamiya et al. 4 with 800 MeV/nucleon Ar+KCl. However, their reactions are inclusive ones, so no detailed comparisons can be made with their work. Figure 9 shows the cross section versus

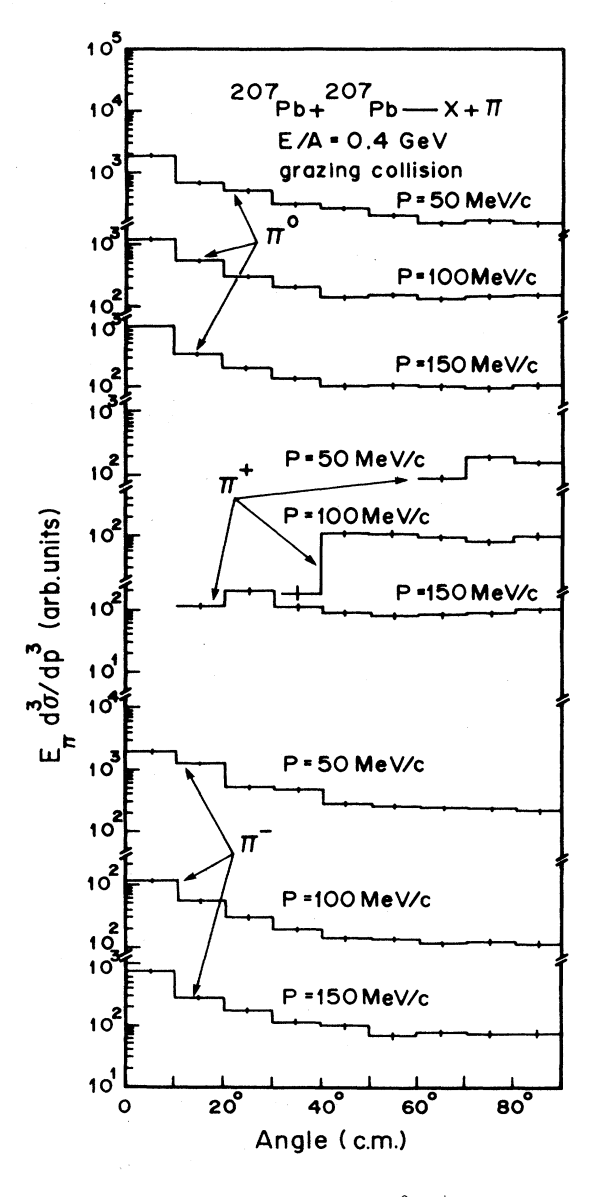


FIG. 9. Differential cross sections for π^0 , π^+ , and π^- resulting from a grazing collision of two ^{207}Pb nuclei in the center-of-mass frame. The cross section is given as a function of pion scattering angle at three pion final momenta (50, 100, and 150 MeV/c).

angle for π^0 , π^+ and π^- at the fixed final momenta 50, 100, and 150 MeV/c. The graphs for the neutral and negative pions show a striking similarity in trend. Also, it is observed that for those pions the cross section decreases for high pion momenta at all angles. The graphs for positive pions show that at pion final momentum of 50 MeV/c, there are no pions found at scattering angles less than 60°. As the momentum is increased, more pions are found at lower angles, until at 150 MeV/c pions have been found at scattering angles as low as 10°. This is again due to the neglect of the quantum effects.

ACKNOWLEDGMENTS

One of us (H.R.) gratefully acknowledges the hospitality and support of the University of California Lawrence Berkeley Laboratory during the course of this work. This work was done with the support of Kuwait University, Grant No. SP029 and Kuwait Foundation for the Advancement of Sciences, Grant No. 87-02-02. Also, support came from the U.S. Department of Energy under Contract No. DE-AC03-76SF00098.

- *Present address: Department of Physics, Indiana University, Bloomington, IN 47405.
- ¹K. L. Wolf, H. H. Gutbrod, W. G. Meyer, A. M. Poskanzer, A. Sandoval, R. Stock, J. Gosset, J.-C. Jourdain, C. H. King, G. King, Nguyen Van Sen, and G. D. Westfall, Phys. Rev. C 26, 2572 (1982).
- ²J. P. Sullivan, J. A. Bistirlich, H. R. Bowman, R. Bossingham, T. Buttke, K. M. Crowe, K. A. Frankel, C. J. Martoff, J. Miller, D. L. Murphy, J. O. Rasmussen, W. A. Zajc, O. Hashimoto, M. Koike, J. Peter, W. Benenson, G. M. Crawley, E. Kashy, and J. A. Nolen, Jr., Phys. Rev. C 25, 1499 (1982).
- ³K. A. Frankel, J. A. Bistirlich, R. Bossingham, H. R. Bowman, K. M. Crowe, C. J. Martoff, D. Murphy, J. O. Rasmussen, J. P. Sullivan, W. A. Zajc, J. P. Miller, O. Hashimoto, M. Koike, J. Peter, W. Benenson, G. M. Crawley, E. Kashy, J. A. Nolen, Jr., and J. Quebert, Phys. Rev. C 25, 1102 (1982).
- ⁴S. Nagamiya, M.-C. Lemaire, E. Moeller, S. Schnetzer, G. Shapiro, H. Steiner, and I. Tanihata, Phys. Rev. C **24**, 971 (1981)
- ⁵W. Benenson, G. Bertsch, G. M. Crawley, E. Kashy, A. Nolen, Jr., H. Bowman, J. G. Ingersoll, J. O. Rasmussen, J. Sullivan, M. Koike, M. Sasao, J. Peter, and T. W. Ward, Phys. Rev. Lett. 43, 683 (1979); 44, 54 (1980).
- ⁶A. Sandoval, H. H. Gutbrod, W. G. Meyer, R. Stock, Ch. Luckner, A. M. Poskanzer, J. Gosset, J.-C. Jourdain, C. H. King, G. King, Nguyen Van Sen, G. D. Westfall, and K. L. Wolf, Phys. Rev. C 21, 1321 (1980).
- ⁷K. L. Wolf, H. H. Gutbrod, W. G. Meyer, A. M. Poskanzer, A. Sandoval, R. Stock, J. Gosset, C. H. King, G. King, Nguyen Van Sen and G. D. Westfall, Phys. Rev. Lett. 42, 1448 (1979).
- ⁸J. Chiba, K. Nakai, I. Tanihata, S. Nagamiya, H. Bowman, J. Ingersoll, and J. O. Rasmussen, Phys. Rev. C 20, 1332 (1979).
- ⁹K. Nakai, J. Chiba, I. Tanihata, M. Sasao, H. Bowman, S. Nagamiya, and J. O. Rasmussen, Phys. Rev. C 20, 2210 (1979).
- ¹⁰J. Miller, J. Bercovitz, G. Claesson, G. Krebs, G. Roche, L. S. Schroeder, W. Benenson, J. van der Plicht, J. S. Winfield, G. Landaud, and J.-F. Gilot, Phys. Rev. Lett. 58, 2408 (1987).
- ¹¹R. B. Clare and D. Strottman, Phys. Rev. C 33, 1288 (1986).
- ¹²A. F. Barghouty and G. Fai, Phys. Rev. C **35**, 950 (1987).
- ¹³J. Miller, Lawrence Berkeley Laboratory Report No. LBL-24275, 1988 (unpublished).
- ¹⁴G. D. Westfall, J. Gosset, P. J. Johansen, A. M. Poskanzer, W. G. Meyer, H. H. Gutbrod, A. Sandoval, and R. Stock, Phys. Rev. Lett. 37, 1202 (1979); J. Gosset, H. H. Gutbrod, W. G. Meyer, A. M. Poskanzer, A. Sandoval, R. Stock, and G. D. Westfall, Phys. Rev. C 16, 629 (1977).

- ¹⁵S. Das Gupta, Phys. Rev. Lett. **41**, 1450 (1978).
- ¹⁶S. Das Gupta and C. S. Lam, Phys. Rev. C 20, 1192 (1979).
- ¹⁷E. Forest, S. Das Gupta, and C. S. Lam, Phys. Rev. C 21, 1989 (1980).
- ¹⁸N. Mobed, S. Das Gupta, and B. K. Jennings, Phys. Rev. C
 27, 1526 (1983); N. Mobed, B. K. Jennings, and S. Das Gupta, Phys. Lett. 106B, 371 (1981); J. Gosset, J. I. Kapusta, and G. D. Westfall, Phys. Rev. C 18, 844 (1978); W. D. Myers, Nucl. Phys. A296, 177 (1978).
- ¹⁹J. Hufner and J. Knoll, Nucl. Phys. **A290**, 460 (1977).
- ²⁰A. A. Amsden, G. F. Bertsch, F. H. Harlow, and J. R. Nix, Phys. Rev. Lett. 35, 905 (1975).
- ²¹A. A. Amsden, J. N. Ginocchio, F. H. Harlow, J. R. Nix, M. Danos, E. C. Halbert, and R. K. Smith, Jr., Phys. Rev. Lett. 38, 1055 (1977).
- ²²A. A. Amsden, A. S. Goldhaber, F. H. Harlow, and J. R. Nix, Phys. Rev. C 17, 2080 (1978).
- ²³J. I. Kapusta and D. Strottman, Phys. Rev. C 23, 1282 (1981).
- ²⁴A. Z. Mekjian, Phys. Rev. Lett. 38, 640 (1977).
- ²⁵A. Z. Mekjian, Phys. Rev. C 17, 1051 (1978).
- ²⁶A. Z. Mekjian, Nucl. Phys. **A312**, 491 (1978).
- ²⁷S. Das Gupta and A. Z. Mekjian, Phys. Rep. **72**, 131 (1981).
- ²⁸C. Gale, A. C. Maso, S. Das Gupta, and B. K. Jennings, Phys. Rev. C 28, 164 (1983).
- ²⁹J. P. Bondorf, H. T. Feldmeier, S. Garpman, and E. C. Halbert, Phys. Lett. 65B, 217 (1976).
- ³⁰J. N. Ginocchio, Phys. Rev. C 17, 195 (1978).
- ³¹Y. Yariv and Z. Fraenkel, Phys. Rev. C 20, 2227 (1979); 24, 488 (1981).
- ³²J. Cugnon, T. Mizutani, and J. Vandermeulen, Nucl. Phys. A352, 505 (1981).
- ³³S. E. Koonin, Phys. Rev. Lett. **39**, 680 (1977).
- ³⁴R. L. Hatch and S. E. Koonin, Phys. Lett. **81B**, 1 (1979).
- ³⁵K. G. Libbrecht and S. E. Koonin, Phys. Rev. Lett. 43, 1581 (1979).
- ³⁶G. Bertsch, Nature **283**, 280 (1980).
- ³⁷J. Cugnon and S. E. Koonin, Nucl. Phys. **A355**, 477 (1981).
- ³⁸M. Gyulassy and S. K. Kauffman, Nucl. Phys. A362, 503 (1981).
- ³⁹J. O. Rasmussen, H. M. A. Radi, K. A. Frankel, J. P. Sullivan, and O. Hashimoto, Lawrence Berkeley Laboratory Report No. LBL-12652-UC-34 Conf-8105-104, p. 397.
- ⁴⁰H. M. A. Radi, J. O. Rasmussen, J. P. Sullivan, K. A. Frankel, and O. Hashimoto, Phys. Rev. C 25, 1518 (1982).
- ⁴¹M. Bawin and J. Cugnon, Phys. Rev. C 25, 387 (1982).
- ⁴²H. M. A. Radi, J. O. Rasmussen, J. P. Sullivan, K. A. Frankel, and H. C. Song Phys. Rev. C 27, 606 (1983).

- ⁴³K. Stricker, H. McManus, and J. A. Carr, Phys. Rev. C 19, 929 (1979).
- ⁴⁴K. Stricker, J. A. Carr, and H. McManus, Phys. Rev. C 22, 2043 (1980).
- ⁴⁵J. A. Carr, H. McManus, and K. Stricker-Bauer, Phys. Rev. C 25, 952 (1982).
- ⁴⁶R. A. Mehrem, H. M. A. Radi, and J. O. Rasmussen, Phys. Rev. C **30**, 301 (1984).
- ⁴⁷D. Jackson, *Nuclear Reactions* (Methuen, New York, 1970), Sec. 6.2.
- ⁴⁸K. M. Watson, Phys. Rev. **89**, 575 (1953).
- ⁴⁹A. K. Kerman, H. McManus, and R. M. Thaler, Ann. Phys.
 (N.Y.) 8, 557 (1959); G. F. Chew, Phys. Rev. 80, 196 (1950);
 G. F. Chew and G. C. Wick, ibid. 85, 636 (1952).
- ⁵⁰M. Ericson and T. E. O. Ericson, Ann. Phys. (N.Y.) 36, 323 (1966).
- ⁵¹L. S. Kisslinger, Phys. Rev. **98**, 761 (1955).
- ⁵²J. A. Carr, Ph.D. thesis, Michigan State University, 1982 (unpublished).

- ⁵³H. M. A. Radi, R. A. Mehrem, and J. O. Rasmussen, Lawrence Berkeley Laboratory Report No. 25639, 1988 (unpublished). An expanded detailed version of this article available on request to NSD Library, 70A-3307, Lawrence Berkeley Laboratory, Berkeley, CA 94720.
- ⁵⁴S. M. Selby, Standard Mathematical Tables, 21st ed. (CRC Press, Boca Raton, FL, 1973), p. 18.
- 55J. P. Sullivan, Ph.D. thesis, University of California, Lawrence Berkeley Laboratory Report No. 12546, 1981 (unpublished).
- ⁵⁶M. M. Sternheim and R. R. Silbar, Phys. Rev. D 6, 3117 (1972).
- ⁵⁷J. O. Rasmussen, in *Proceedings of the International Symposium on Nuclear Spectroscopy and Nuclear Interactions, Osaka, 1984* edited by H. Ejiri and T. Fukuda (World Scientific, Singapore, 1984).
- ⁵⁸R. R. Silbar and M. M. Sternheim, Phys. Rev. C 8, 492 (1973).
- ⁵⁹D. S. Beder and P. Bendix, Nucl. Phys. **B26**, 597 (1971).